Theoretical Investigation on Semiconductor Lasers with Passive Waveguides

Shun Tung Yen, *Student Member, IEEE*, and Chien Ping Lee, *Senior Member, IEEE*

***Abstract*—Semiconductor lasers with vertically integrated passive waveguides are theoretically studied using the coupled mode theory and exact calculation. Formulas for the threshold current density and the far-field patterns are derived. The physical concepts of the modulation of the beam divergence by passive waveguides are given. The exact caluclated results show that the beam divergence can be greatly improved by paying a price of only a slight increase of the theshold current density. The operation mode selection is discussed. Attention is also paid to the appearance of side lobes for very narrow far-field patterns. Discussions are given for device design.**

I. Introduction

THE BEAM property of a laser diode is of great importance whenever the laser output is needed to be coupled into another device. For lasers used to optically pump Er^{3+}-doped fiber amplifiers (EDFA), high coupling efficiency is particularly important because high pumping power is needed for the operation of the amplifiers [1]. To obtain high-power coupling, required are not only the high output power but also a narrow beam divergence. There have been a large amount of reports on low threshold current [2]–[4] and high output power [5]–[7] InGaAs–AlGaAs pump lasers at wavelength of 980 nm. However, in conventional graded-index separate confinement heterostructure (GRINSCH) quantum well lasers, the tight optical confinement causes a large beam divergence in the direction perpendicular to the heterojunction. This results in highly asymmetric elliptical far-field patterns and, therefore, reduces the coupling efficiency. This problem can be cured by expanding the size of the transverse electric field in the optical cavity. Furthermore, an expanded electrical field distribution reduces the risk of mirror damage at high power operations and therefore increases the laser's life time. Structures for this purpose include the large optical cavity and the thin active layer [8]. However, reduction of the beam divergence for these structures is limited and usually accompanied by a significant increase of the threshold current.

Recently, lasers with very small beam divergence have been achieved by engineering the cladding layers [9]–[13]. Wu *et al.* utilized periodic-index confining layers to replace the conventional cladding layers and achieved high power coupling into a fiber[9]. Cockerill *et al.* used a depressed index cladding graded barrier structure to obtain a large size Gaussian-like mode [10]. A reduced beam divergence was achieved with acceptable low-threshold current density. These structures involve the engineering of the blocking behavior of cladding layers. Different from these two approaches. Chen *et al.* integrated passive waveguides in the cladding layer and obtained a low-beam divergence of 11.2° [13]. In spite of the improved performance, the danger of the emission of a higher-order mode may occur, which results in side lobes in the far-field pattern and degrades the beam divergence. Besides, even in the fundamental mode operation, the extremely small beam divergence is usually accompanied with obvious side lobes for these lasers.

In this paper, we theoretically investigate in detail the performance of the lasers with passive waveguides in the cladding layers. In the following section, the coupled mode theory is used to demonstrate the physical concept of the reduction of the beam divergence due to the existence of passive waveguides. Formulas for both the threshold current density and the far-field patterns are derived. In Section III, we give the exact calculated results of the threshold current density and the beam divergence for the coupled waveguide lasers. The formulas derived in Section II are used to interpret the calculated results. Greatly improved beam divergence can be achieved at the expense of only a slight increase of the threshold curent density. We discuss the threshold mode selection and the problem of the appearance of side lobes for small far-field patterns. A description is also given for the influence of material quality and the longitudinal optical cavity length on the threshold current density for the coupled waveguide lasers. Discussions are given in Section IV from the viewpoint of device design. Finally, we conclude this work in Section V.

II. Theoretical Analysis

The conventional coupled mode theory [14] is used here to illustrate the physical picture of how the passive waveguides influence the performance of semiconductor lasers. We consider the laser structure shown in Fig. 1 with a conventional GRINSCH active waveguide (denoted as waveguide 2) and two subordinate waveguides (denoted as waveguides 1 and 3). This structure is similar to the coupled waveguide structure proposed in [15] but the active waveguide in our structure contains a thin quantum well that provides gain for the laser operation. The subordinate waveguides are passive, i.e., there is no gain in these regions. Assuming the coupled structure is symmetric and according to the simple coupled mode theory,

Manuscript received April 17, 1995; revised August 29, 1995. This work was supported by the National Science Council of the Republic of China under Contract NSC84-2215-E009-039.

The authors are with the Department of Electronics Engineering, National Chiao Tung University, Hsinchu 300, Taiwan, R.O.C.

Publisher Item Identifier S 0018-9197(96)00337-5.

the transverse electric fields in the coupled structure can be written in linear combination of individual uncoupled electric fields $\psi_1(x)$, $\psi_2(x)$, and $\psi_3(x)$ for waveguides 1, 2, and 3, respectively. The resulting effective refractive indices (defined as the propagation constant along the waveguide divided by that in free space k_0) for the three guided modes can be approximated as

$$\eta_{\text{eff}+} = \frac{1}{2}[n_{\text{eff}1} + n_{\text{eff}2} + \sqrt{(n_{\text{eff}1} - n_{\text{eff}2})^2 + 8\kappa^2}] \quad (1)$$

$$n_{\text{eff}} = n_{\text{eff}2} \quad (2)$$

$$n_{\text{eff}-} = \frac{1}{2}[n_{\text{eff}1} + n_{\text{eff}2} - \sqrt{(n_{\text{eff}1} - n_{\text{eff}2})^2 + 8\kappa^2}], \quad (3)$$

where $n_{\text{eff}1}$ and $n_{\text{eff}2}$ are the effective refractive indices for uncoupled waveguides 1 and 2, respectively. κ is the coupling coefficient proportional to the overlap integral of electric fields $\psi_1(x)$ and $\psi_2(x)$. The resulting transverse electric field in the coupled structure is

$$\psi(x) = \sum_{i=1}^{3} a_i \psi_i(x). \quad (4)$$

The three guided eigenmodes have different a_i's, which are expressed by the following vectors:

$$[a_1 a_2 a_3]_+ = [2 + (c+d)^2]^{-\frac{1}{2}}[1 \quad c+d \quad 1] \quad (5)$$

$$[a_1 a_2 a_3] = 2^{-\frac{1}{2}}[1 \quad 0 \quad -1] \quad (6)$$

$$[a_1 a_2 a_3]_- = [2 + (c-d)^2]^{-\frac{1}{2}}[1 \quad c-d \quad 1] \quad (7)$$

where

$$c = \frac{n_{\text{eff}2} - n_{\text{eff}1}}{2\kappa} \quad (8)$$

$$d = \sqrt{c^2 + 2}. \quad (9)$$

Clearly, because $c + d > 0$ and $c - d < 0$, (5), (6), and (7) belong, respectively, to the fundamental, the first-order, and the second-order modes. For the fundamental mode the electric field tends to concentrate in the waveguide with a larger effective refractive index. On the other hand, for the second-order mode, the electric field has a tendency to concentrate in the waveguide with a smaller effective reflective index. For the first-order mode, because there is a node in waveguide 2, the electric field is nearly zero there.

The confinement factor for the coupled structure can be approximated as

$$\Gamma = \psi^2(0)w, \quad (10)$$

where the center of symmetry of the structure is at $x = 0$. We have assumed that the modes are normalized and the quantum well (with thickness of w) is very thin so that the electric field is nearly constant in the region. Similarly, if the passive waveguides do not exist, the confinement factor for the uncoupled structure is

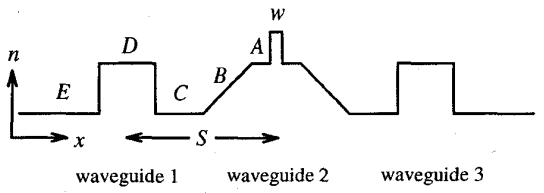

Fig. 1. The coupled waveguide structure with an active and two passive waveguides.

$$\Gamma_2 = \psi_2^2(0)w. \quad (11)$$

Inserting (4) into (10) and using the fact

$$a_2^2\psi_2^2(0) \gg a_1^2\psi_1^2(0), \quad (12)$$

we obtain

$$\Gamma_\pm = \left[1 + \frac{2}{(c \pm d)^2}\right]^{-1}\Gamma_2, \quad (13)$$

where Γ_+ and Γ_- are confinement factors for the fundamental and the second-order modes. The confinement factor for the first-order mode is nearly zero because the electric field is nearly zero in the quantum well. The threshold mode selection for the coupled waveguide laser is determined by the confinement factors. From (8), (9), and (13), it is found that to obtain a fundamental mode emission (under the condition $\Gamma_+ > \Gamma_-$), $n_{\text{eff}2}$ has to be larger than $n_{\text{eff}1}$.

The threshold current density for quantum-well lasers can be well approximated as the exponential expression [16]

$$J_{\text{th}} = \frac{J_0}{\eta_i}\exp\left(\frac{\alpha_t}{\Gamma b_0 J_0}\right), \quad (14)$$

where J_0 is the transparency current density, η_i the internal quantum efficiency, b_0 the gain coefficient, and α_t the total loss including the mirror loss and all internal material losses. The expression (14) can be well fitted to experimental data, and parameters such as J_0 and b_0 are obtained by the fitting. All parameters except Γ and α_t depend only on the thicknesses of the quantum well and the barriers (denoted as w and A, respectively in Fig. 1) but are independent of whether the passive waveguides exist or not [17]. The total loss α_t, although depending on the cladding materials, can be regarded as a constant and independent of the existence of the passive waveguides. This is because the existence of passive waveguides causes only a very small amount of increase in material loss. The published experimental data showed that the material loss is usually smaller than 10 cm^{-1} for InGaAs–AlGaAs lasers. Extremely low loss smaller than 2 cm^{-1} has been reported [3], which is much smaller than the mirror loss which is the dominant loss mechanism for most laser structures. Therefore, using (13) and (14), the threshold current density for the coupled structure is

$$J_{\text{th}}^{\pm} = J_{\text{th}2}\exp\left[\frac{2}{(c \pm d)^2}\frac{\alpha_t}{\Gamma_2 b_0 J_0}\right]. \quad (15)$$

Γ_2 and $J_{\text{th}2}$ represent the confinement factor and the threshold current density for the structure without passive waveguides. J_{th}^+ and J_{th}^- are the threshold current densities for the emission of the fundamental mode and the second-order mode, respectively. Clearly, based on this equation, because the exponent is always positive, the threshold current density for the coupled structure is always larger than that for the structure without passive waveguides. Because of the exponential expression, the threshold current density can remain insensitive to the confinement factor and the coupling between waveguides (through $c \pm d$) if the argument of the exponential function is small. On the other hand, when the argument of the exponential function is large compared to unity, the threshold current density will be very sensitive to both the confinement factor and the coupling between the waveguides.

The far-field pattern can be obtained by taking the Fourier transformation of the near-field distribution. The field strength in free space at angle Θ is written as [8]

$$\phi(\Theta) = G(r)g(\Theta)\int_{-\infty}^{\infty} \psi(x)\exp(ik_0 x \sin\Theta)\,dx, \qquad (16)$$

where $G(r)$ is independent of the far-field angle Θ. $k_0 = 2\pi/\lambda$ is the free space propagation constant. $g(\Theta)$ is the Huygen's correction factor for which several expressions are available. The best choice according to [18] is

$$g(\Theta) = \frac{\cos\Theta}{\cos\Theta + n_{\text{eff}}}. \qquad (17)$$

By inserting (4) into (16) and after some simplification, we obtain the far field for the coupled structure

$$\frac{\phi_{\pm}(\Theta)}{\phi_{\pm}(0)} = M_{\pm}\frac{\phi_1(\Theta)}{\phi_1(0)}\cos(k_0 S\sin\Theta) + (1 - M_{\pm})\frac{\phi_2(\Theta)}{\phi_2(0)}, \qquad (18)$$

where $M_{\pm}$, we call the *modulation factors*, are defined as

$$M_{\pm} = \left[1 + \frac{c \pm d}{2}\frac{\phi_2(0)}{\phi_1(0)}\right]^{-1}. \qquad (19)$$

$\phi_1(\Theta)$ and $\phi_2(\Theta)$ are the far fields belonging to waveguides 1 and 2, respectively. $\phi_+(\Theta)$ and $\phi_-(\Theta)$ result respectively from the fundamental and the second-order modes. S, as shown in Fig. 1, is the separation between neighboring waveguides. An interesting result from (18) is that the output electric field from the coupled structure is composed of that from waveguide 2 modulated by those from waveguides 1 and 3 through the modulation factor and the waveguide separation S. The modulation factor determines the weight of mixing between $\phi_1(\Theta)$ and $\phi_2(\Theta)$. When the coupling between waveguides is very weak, the values of M_+ for the fundamental mode ($n_{\text{eff}2} > n_{\text{eff}1}$) and M_- for the second-order mode ($n_{\text{eff}1} > n_{\text{eff}2}$) approach zero [as can be seen from (8), (9), and (19)] and then the contribution to the far field almost comes entirely from the waveguide 2. The modulation of the beam divergence by the passive waveguides is therefore inefficient. S, contained in the argument of the cosine function, plays an important role in the shape of the far-field pattern. Fig. 2 illustrates how $M_{\pm}$ and S work. In this illustration, we assume that the far-field patterns for waveguides 1 and 2, ϕ_1 and ϕ_2, are the same [shown in Fig. 2(a)]. In Fig. 2(b), we show the plot of $\cos(k_0 S\sin\Theta)$ versus Θ for $k_0 S = 1$, 5, and 10. We see that for a small $k_0 S$ the function $\cos(k_0 S\sin\Theta)$ varies slowly with Θ and the pattern is wide. On the other hand, for a large $k_0 S$, $\cos(k_0 S\sin\Theta)$ varies rapidly with Θ and the lobes are narrow. Fig. 2(c) shows the final modulated far-field patterns for $k_0 S = 1$, 5, and 10. For the fundamental mode, because $0 < M_+ < 1$ (where M_+ is chosen as 0.5), the two terms in the right hand side of (18) have the same sign for $\Theta = 0$ and then the beam divergence can be significantly improved due to the presence of the passive waveguides. We also find that a larger $k_0 S$ causes a smaller beam divergence. However, side lobes appear. This is because the rapid variation of $\cos(k_0 S\sin\Theta)$ with Θ for a large $k_0 S$ and the width of the central lobe for $\cos(k_0 S\sin\Theta)$ is much narrower than that of the unmodulated field shown in Fig. 2(a). On the other hand, when $k_0 S$ is small, the modulation is inefficient because of the weak angular dependence of $\cos(k_0 S\sin\Theta)$. The far field is then comparable to that of the unmodulated field. A compromise can be reached by taking $k_0 S = 5$. It can be seen that for $k_0 S = 5$ the beam divergence has been much improved and the problem of side lobes is not serious.

When the lasing mode is the second-order mode, the modulation factor $M_- > 1$ or $M_- < 0$. The beam divergence will be poor because the two terms in the right-hand side of (18) have opposite signs for $\Theta = 0$ and the field strength around $\Theta = 0$ is reduced.

III. Numerical Results

The simple couple mode theory is a useful tool for a qualitative understanding of the interaction between waveguides. However, because of the assumption of weak coupling, it is not suitable for the quantitative calculation when the coupling is strong. In this section exact numerical results are presented for the beam divergence and the threshold current density. Comprehensible interpretation is given for these results using the coupled mode theory.

In the calculation, only TE waves are considered. The structures treated are InGaAs–AlGaAs strained GRINSCH laser for 980 nm emission applications. Fig. 1 has shown this kind of structures, which is composed of $Al_xGa_{1-x}As$ in regions C and E, GaAs regions A and D, $In_{0.2}Ga_{0.8}As$ in the quantum-well region w, and the linearly graded AlGaAs in region B. The well and barrier thicknesses are chosen as $w =$ 65 Å and $A =$ 150 Å. the transfer matrix method is used to calculate the guided modes [16]. In calculating the threshold current density, formula (14) is used. The parameters used in calculation are $J_0 = 50$ A/cm^2, $b_0 = 24$ cm/A, $\eta_i = 0.97$, and $\alpha_t = 20$ cm^{-1} for a 1-mm-long cavity and a material loss of 7 cm^{-1} [16]. The far-field patterns are calculated using formulas (16) and (17). The refractive indices of AlGaAs and GaAs used in the calculation are obtained from Casey and Panish [8].

Fig. 3 shows the calculated confinement factor, the threshold current density, and the full width at half maximum (FWHM) of the far field versus the thickness of the graded

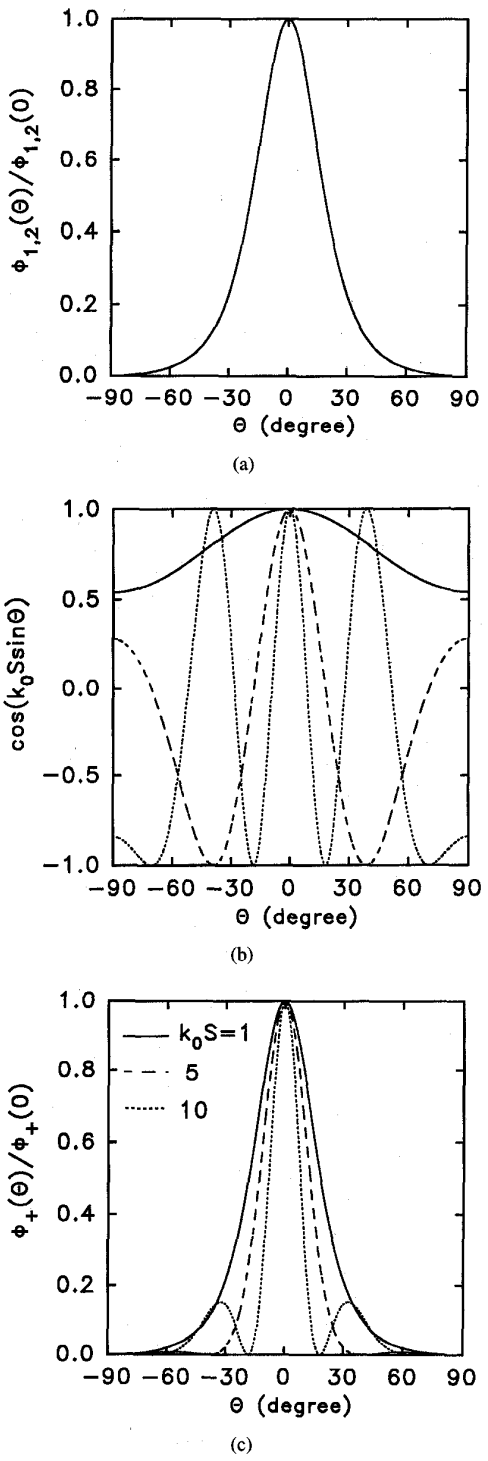

Fig. 2. (a) The strength of far fields for waveguides 1 and 2, ϕ_1 and ϕ_2 versus the observation angle Θ. We assume $\phi_1 = \phi_2$. (b) The plot of $\cos(k_0 S \sin\Theta)$ versus Θ. (c) The strength of far fields for coupled waveguide structures versus Θ. The emission of the fundamental mode is assumed and $M_+ = 0.5$. In (b) and (c) we consider $k_0 S = 1$ (the solid line), $k_0 S = 5$ (the dashed line), and $k_0 S = 10$ (the dotted line).

region B for conventional lasers without passive waveguides ($D = 0$), with the AlAs molar fraction x in region C as the parameter. The confinement factor shown in Fig. 3(a), as the well-known result [8], increases rapidly with B to reach the maximum and then decreases slowly. The reason is the cavity-size effect. Both large and small transverse optical cavities cause the expansion of the transverse electric fields and then reduce the confinement factor. For a small Al composition x, because the small difference between the refractive indices in A and C causes the expansion of the electric field, the confinement factor is reduced. In Fig. 3(b), the threshold current density, which is related to the confinement factor through (14), increases drastically when B is smaller than 1000 Å. So very small B should be avoided. Due to the cavity-size effect, the threshold current density has a minimum and increases slowly with B. Fig. 3(c) shows the calculated FWHM for the structures described above. Small FWHM's are always obtained for structures with small B's and x's. This is because, for smaller B's and x's, the electric field has a wider spread. Unfortunately, the small beam divergence is always obtained together with a high threshold current density. It can be seen from Fig. 3(b) and (c) that to obtain a beam divergence smaller than 30°, a price has to be paid with a much increased threshold current density. The trade-off between the threshold current density and the beam divergence is obviously tight for a conventional GRINSCH laser.

The tightness of the trade-off between the threshold current density and the beam divergence can be cured by the addition of passive waveguides to cladding layers, which provides an additional degree of freedom in device design. Fig. 4 shows the calculated threshold current density and the beam divergence versus the thickness C for structures with passive waveguides. In these structures, the Al composition x in region C is taken to be 0.4 and the thickness of the graded region, B is chosen as 800 Å. Three different thicknesses for the passive waveguides, $D = 0$, 500, and 1000 Å, were considered in the calculation. For these passive and active waveguides described above, the lasing mode is the fundamental mode ($n_{\text{eff2}} > n_{\text{eff1}}$). From Fig. 4(a), we find that for the coupled waveguide structrues the threshold current density has a maximum at some C and decreases with both the increase and decrease of C. When C is large, i.e., the separation between waveguides is large, the coupling between waveguides is very small. As can be found from (8) and (9), for $n_{\text{eff2}} > n_{\text{eff1}}$, $c + d$ approaches infinity when the coupling coefficient κ approaches zero. The threshold current density for the coupled waveguide laser J_{th}^+ therefore approaches that without the passive waveguides [see (15)]. On the other hand, when C is very small, the coupling between waveguides becomes large and the results derived from the coupled mode theory are no longer valid. We can interpret the behavior of the threshold current density as follows. Because of the very small separation between the waveguides, the electric field will concentrate around the active waveguide. The confinement factor and, therefore, the threshold current density approach the values for the structure without passive waveguides. It can be also found from Fig. 4(a) that for thicker passive waveguides, the threshold current density is higher. This is caused by two origins. The major one is that a thicker passive waveguide (region D) contains a larger amount of electric field

than a thinner one, resulting in a smaller cofinement factor and, therefore, a higher threshold. Another origin can be explained as follows. Because for $D = 1000$ Å n_{eff1} is closer to n_{eff2} than for $D = 500$ Å, $c + d$ is smaller for $D = 1000$ Å. Based on (15), a smaller $c + d$ results in a higher threshold current density.

Fig. 4(b) shows the calculated FWHM versus C for the structures described above. Much improved beam divergence can be achieved for $D = 1000$ Å. As will be seen below, because the far-field pattern for $D = 1000$ Å is modulated more efficiently than for $D = 500$ Å, the FWHM for $D = 1000$ Å is therefore more improved than for $D = 500$ Å. By comparing Fig. 4(b) with Fig. 4(a), one can find that an FWHM smaller than 30° can be easily obtained with only a slight increase of the threshold current density. For example, when $C = 8700$ Å and $D = 1000$ Å, an FWHM of 21° is achieved along with a threshold current density of 160 A/cm^2. For $C = 10\,200$ Å and $D = 1000$ Å, we have FWHM = 23 °C and $J_{\text{th}} = 144\ A/\text{cm}^2$. Clearly, these results are superior to those for the structure without passive waveguides, which have FWHM = 38° and $J_{\text{th}} = 136\ A/\text{cm}^2$ (see Fig. 3).

As described in the previous section, side lobes may appear when the separation between waveguides is large. The side lobes can lower the optical power coupling to another device. Therefore a small FWHM, without considering the side lobes, does not necessarily mean a good beam divergence. A more reasonable definition for the beam divergence is the full width *containing* the half power (FWCHP) which is defined as

$$\frac{\int_{-\frac{1}{2}\text{FWCHP}}^{\frac{1}{2}\text{FWCHP}} |\phi(\Theta)|^2\, d\Theta}{\int_{-\frac{\pi}{2}}^{\frac{\pi}{2}} |\phi(\Theta)|^2\, d\Theta} = \frac{1}{2}. \tag{20}$$

Fig. 4(c) is the plot of FWCHP versus C for these structures described above. By comparing Fig. 4(c) with 4(b), we find that FWCHP is not improved as much as FWHM for C's larger than 1 μm. This is due to the appearance of side lobes caused by the larger separation between the waveguides.

From Fig. 4(b), we can find an obvious oscillation of FWHM, which is caused by the cosine function $\cos(k_0 S \sin\Theta)$. The period for the oscillation is estimated to be about $2\pi/k_0 \sin\Theta = \lambda/\sin\Theta \approx 0.23$ μm if we choose $\Theta \approx 25°$. The estimated period is in agreement with the calculated result shown in figures. The oscillation is also obvious in the plot for FWCHP [Fig. 4(c)]. On the other hand, in Fig. 4(a), the threshold current density lacks such oscillation. In device design, it is thus desirable to choose a C so that a local minimum of FWCHP is obtained while the threshold current density remains small.

Only the fundamental modes are considered for the structures treated so far (for $D \leq 1000$ Å). However, when D becomes very large, the effective refractive index n_{eff1} can be larger than n_{eff2}. As can be seen from (8), (9), and (13), the confinement factor for the second-order mode is then larger than that for the fundamental mode. In this situation, the second-order mode becomes the lasing mode and then poor beam divergence results.

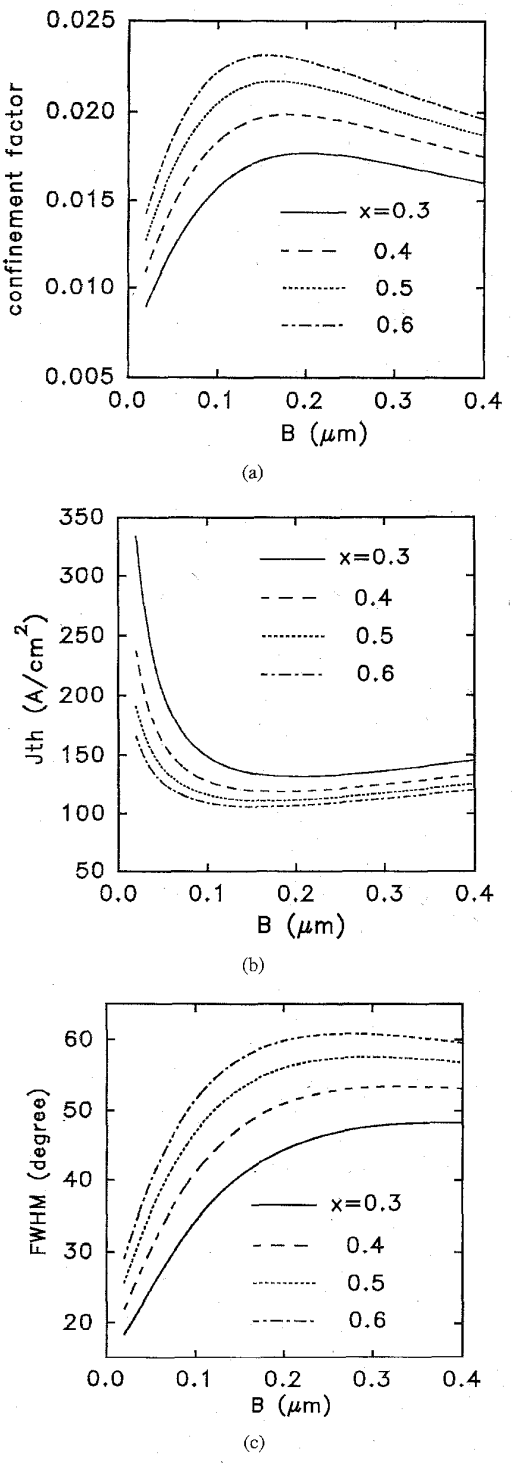

Fig. 3. Plots of (a) the confinement factor, (b) the threshold current density, and (c) FWHM versus B for conventional InGaAs–AlGaAs GRINSCH lasers lacking passive waveguides. In these structures, $A = 150$ Å and $w = 65$ Å. The solid line is for an AlAs molar fraction $x = 0.3$ in region C, the dashed line for $x = 0.4$, the dotted line for $x = 0.5$, and the dash-dotted line for $x = 0.6$.

Fig. 5 shows the effect of the operation of the second-order mode on the lasing characteristics. The plots are similar to Fig. 4 but results for wider passive waveguides ($D = 1200$

and 1600 Å) are included. Fig. 5(a) shows the dependence of the threshold current density on C with various thicknesses of passive waveguides. Again as expected, we see that the threshold current density increases with D because a thicker D reduces the confinement factor. Fig. 5(b) shows the plot of FWHM versus C. In this figure, there is a considerable dissimilarity between the results for $D > 1000$ Å and those for $D \leq 1000$ Å. For $D > 1000$ Å, the FWHM abruptly hops to a maximum value when C reaches a critical thickness C_c ($C_c \approx 2000$ Å in this figure). The sudden deterioration in beam divergence is due to the switching of the lasing mode from the fundamental mode to the second-order mode. However, before C reaches the critical value C_c, even for a large D ($n_{\text{eff}1} > n_{\text{eff}2}$), the FWHM remains small because the fundamental mode still prevails. This can be seen from (3), because of strong coupling between waveguides, $n_{\text{eff}-}$ becomes so small that the second-order mode can not be guided. In spite of the acceptable FWHM in this case, it can be seen from Fig. 5(a) that the threshold current density is unacceptably large since the electric field tends to concentrate in the passive waveguides for the fundamental mode when $n_{\text{eff}1} > n_{\text{eff}2}$.

From Fig. 5(b), it is expected that there exists a critical thickness of D, denoted as D_c, between 1000 Å and 1200 Å, where $n_{\text{eff}1}$ and $n_{\text{eff}2}$ cross over ($n_{\text{eff}1} = n_{\text{eff}2}$) and $|c \pm d|$ reaches the minimum. For $D < D_c$, the FWHM is reduced with increasing D because of the decrease of $|c + d|$ and then the increase of the modulation factor [see (18) and (19)]. One can see from the plots of FWHM and FWCHP that the improvement in the beam divergence is small for both too small and too large C's. For large C's, the modulation factor is small due to the weak coupling between the waveguides, while for small C's, i.e., small separation S between waveguides, the angular dependence of $\cos(k_0 S \sin\Theta)$ becomes weak resulting in inefficient modulation.

When C becomes very large, the coupling between waveguides becomes very weak and the performance of the coupled structures converges to that of the structure without passive waveguides. When $n_{\text{eff}1}$ is closer to $n_{\text{eff}2}$, for example, when $D = 1000$ or 1200 Å, the convergence is slow with the increase of C. According to (8) and (9), for small $|n_{\text{eff}1} - n_{\text{eff}2}|$, one needs a much small coupling coefficient κ and thus a much large C to obtain a large $|c \pm d|$. This slow convergence makes possible the efficient modulation of the far-field pattern using a large separation S, i.e., the modulation factor can be large accompanied with a large separation S.

Fig. 6 shows the plots of the threshold current density, FWHM, and FWCHP for the coupled waveguide structures as functions of the thickness D. As before, $A = 150$ Å, $B = 800$ Å, $w = 65$ Å, and the Alas molar fraction x in the C regions is 0.4. Three different thicknesses for region C, $C = 4000$, 8000, and 16 000 Å were considered in the calculation. Impacts of the change of the threshold mode are clearly shown in these figures. As can be seen in Fig. 6(a), there are sharp peaks of the threshold current density at the critical D_c. When $D = D_c$, the confinement factor for the threshold mode is at the minimum because the confinement factors for both of the

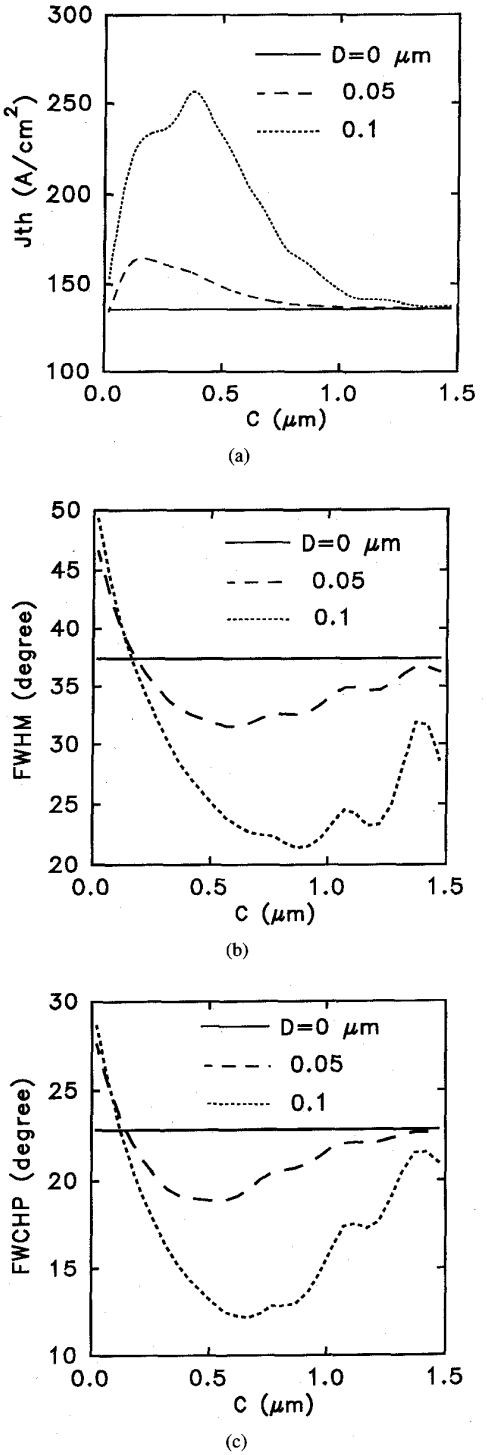

Fig. 4. Plots of (a) the threshold current density, (b) FWHM, and (c) FWCHP versus C for structures with $A = 150$ Å, $B = 800$ Å, $w = 65$ Å, and the AlAs molar fraction x in region C is 0.4. The solid line is for $D = 0$, the dashed line for $D = 500$ Å, and the dotted line for $D = 1000$ Å.

fundamental mode and the second-order mode cross over in this situation. The width of the resonance peak is narrower for a larger C. This result can be easily understood by utilizing the coupled mode theory. For a larger C, the coupling coefficient

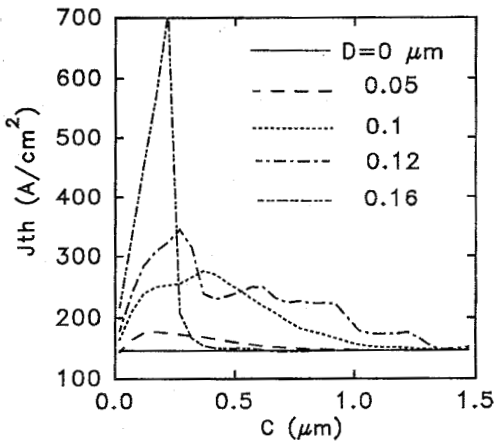

(a)

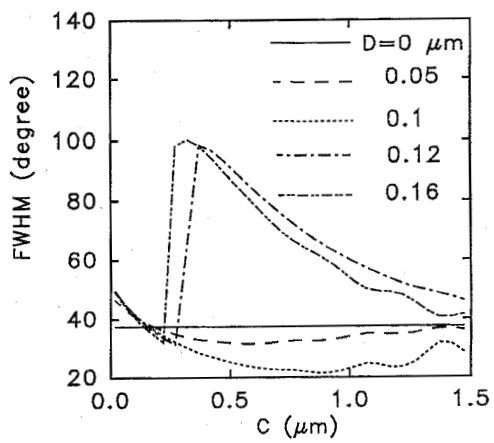

(b)

Fig. 5. Plots of (a) the threshold current density and (b) FWHM versus C for structures with $A = 150$ Å, $B = 800$ Å, $w = 65$ Å, and the AlAs molar fraction x in region C is 0.4. The solid line is for $D = 0$, the dashed line for $D = 500$ Å, the dotted line for $D = 1000$ Å, the dash-dotted line for $D = 1200$ Å, and the dash-dot-dotted line for $D = 1600$ Å.

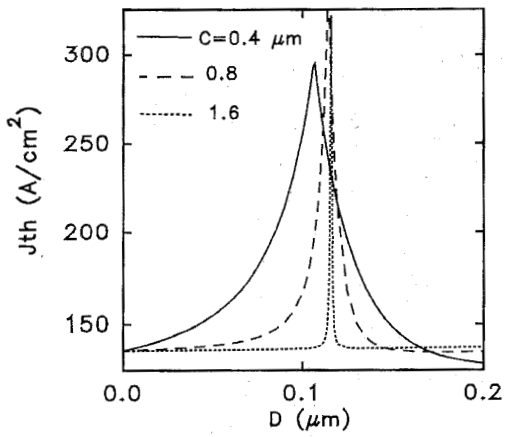

(a)

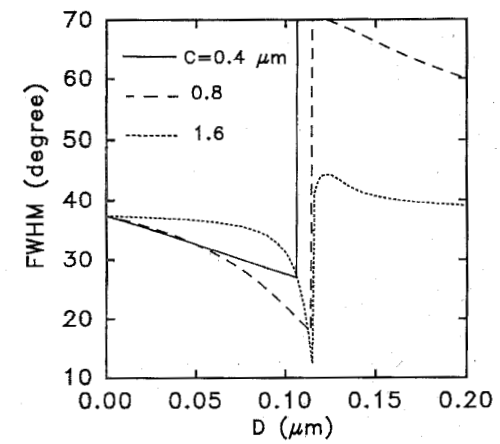

(b)

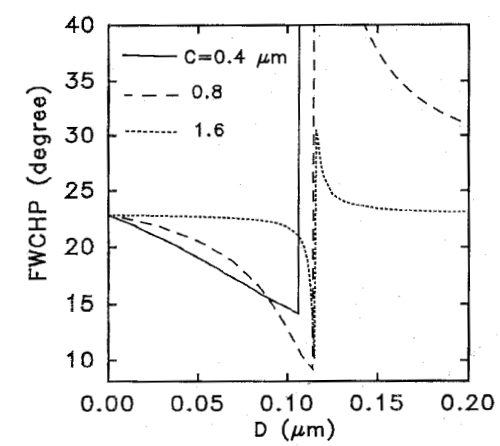

(c)

Fig. 6. Plots of (a) the threshold current density, (b) FWHM, and (c) FWCHP versus D for the coupled waveguide structures with $A = 150$ Å, $B = 800$ Å, $w = 65$ Å, and the AlAs molar fraction x in region C is 0.4. The solid line is for $C = 4000$ Å, the dashed line for $C = 8000$ Å, and the dotted line for $C = 16000$ Å.

κ is smaller and $|c+d|$ ($|c-d|$) is larger for the fundamental mode (the second-order mode). From (15), one can see that the threshold current density for a larger C (larger $|c \pm d|$) is lower than that for a smaller C (smaller $|c \pm d|$) except when D approaches the critical value D_c ($n_{\text{eff1}} \approx n_{\text{eff2}}$). This makes the resonance peak of the threshold current density narrower for a larger C. As will be seen in the following, the narrow peak of threshold current density allows us to choose a D close to D_c, at which the threshold current density remains small but a significantly improved FWHM can be achieved. It is found that for D larger than about 1700 Å, the threshold current density for smaller C can be lower than that for larger C. This is in contradiction to the expectation from the coupled mode theory (15). The behavior, similar to Fig. 3(b), is the optical cavity effect. This effect becomes innegligible when the coupling is strong.

Fig. 6(b) is the plot for FWHM. We see that the FWHM decreases with D and then reaches the minimum at $D = D_c$. As expected, when D crosses over D_c, the lasing mode switches from the fundamental mode to the second-order mode and the FWHM abruptly hops from the minimum to the maximum. FWHM lower than 20° can be obtained when D

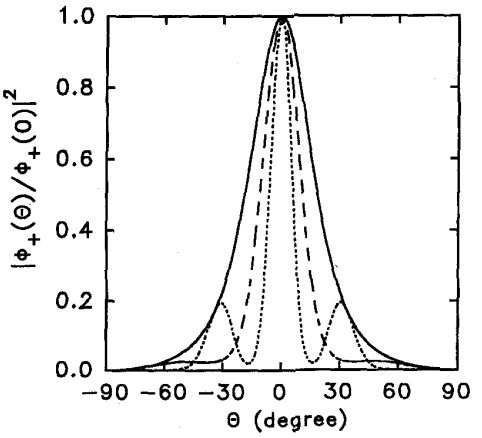

Fig. 7. The far-field patterns for structures with $A = 150$ Å, $B = 800$ Å, $w = 65$ Å, and the AlAs molar fraction x in region C is 0.4. The solid line is for $D = 0$ (lacking the passive waveguides), the dashed line for $C = 8000$ Å and $D = 1000$ Å, and the dotted line for $C = 16000$ Å and $D = 1050$ Å.

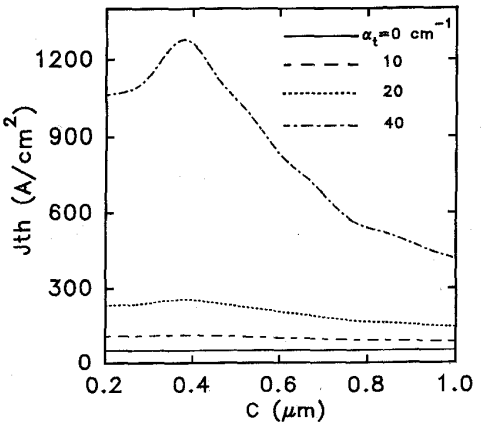

Fig. 8. The threshold current density versus C for structures with $A = 150$ Å, $B = 800$ Å, $D = 1000$ Å, $w = 65$ Å, and the AlAs molar fraction x in region C is 0.4. The solid line is for $\alpha_t = 0$, the dashed line for $\alpha_t = 10$ cm^{-1}, the dotted line for $\alpha_t = 20$ cm^{-1}, and the dash-dotted line for $\alpha_t = 40$ cm^{-1}.

is around D_c. By comparing Fig. 6(a) with Fig. 6(b), we see that a considerable improved FWHM can be achieved with a slight increase of the threshold current density. For larger C's, the dip at the minimum of FWHM is sharper. This can be interpreted by the reason similar to that for the relation between the resonance peak width of the threshold current density and the thickness of region C. For a smaller coupling coefficient κ, the modulation factor M_+ is smaller. A smaller minimum FWHM can be achieved for a larger C due to the narrow central lobe of the cosine function $\cos(k_0 S \sin\Theta)$ (see Fig. 2). However, in spite of the extremely small FWHM, if the dip around $D = D_c$ is too sharp, the region for small FWHM becomes so narrow that the tolerance to obtain a small FWHM is tight. Even if a much smaller FWHM is available, it does not mean it is a desired pattern because of the appearance of side lobes for large C's. In this case, we prefer FWCHP to FWHM for the judgment of the beam divergence. Fig. 6(c) is the plot for FWCHP. The behavior for FWCHP is generally similar to that for FWHM. The main difference is that the smallest minimum FWCHP occurs at $C = 8000$ Å rather than at $C = 16000$ Å. The beam divergence clearly becomes undesirable for large C's. To demonstrate that the use of FWCHP is more suitable than that of FWHM, we plot the far-field patterns for three different structures in Fig. 7. Although the far-field pattern for the structure with $C = 16000$ Å and $D = 1050$ Å has an FWHM as low as 12°, the problem of side lobes is serious. On the other hand, the far-field pattern with an FWHM of 22° for the structure with $C = 8000$ Å and $D = 1000$ Å lacks such serious side lobes. The beam divergence for this structure is clearly superior to that for $C = 16000$ Å and $D = 1050$ Å and to that for the structure without the passive waveguides. This is in agreement with the result of FWCHP in Fig. 6(c) which implicitly considers the shape of the far-field pattern.

When calculating the threshold current density, we have assumed that the parameters in the argument of the exponential function in (14) are constant except the confinement factor Γ. It is worthy to investigate the influence of these parameters on the performance of a coupled waveguide laser. Fig. 8 is the plot for the threshold current density versus C with the total loss α_t as a parameter. The structures considered are with $A = 150$ Å, $B = 800$ Å, $D = 1000$ Å, $w = 65$ Å, and the AlAs molar fraction x for the C regions is 0.4. As can be seen, when C is small, the coupling between waveguides is strong and the threshold current density rises. The threshold current density is sensitive to the coupling between the waveguides for large losses such as $\alpha_t = 40$ cm^{-1}. Because the loss is contributed mainly from the mirror loss, a long cavity of low mirror loss is desired for the coupled waveguide laser. For a cavity length of 1 mm, which we have considered in this study, the total loss $\alpha_t = 20$ cm^{-1} and the threshold current density remains weakly dependent on the coupling. On the other hand, if the cavity length is chosen to be 300 μm, the total loss α_t is about 40 cm^{-1}, resulting in the increase sensitivity of the threshold current density to the coupling strength.

IV. Discussion

We have found that two more parameters C and D can be utilized in device design for coupled waveguide lasers than for conventional lasers. The tightness of trade-off between current density and beam divergence for the conventional laser can be overcome by these addditional degrees of freedom. We have known that the coupled waveguide laser can be used to significantly improve the beam divergence at only a small sacrifice of the threshold current density when the parameters, such as the thicknesses of regions B, C, and D, the AlAs molar fraction x, and the longitudinal optical cavity length, are properly chosen.

When designing a coupled waveguide laser, it is of the most importance to make sure that n_{eff1} is never larger than n_{eff2} for the operation of the fundamental mode. The second-order mode causes poor beam divergence. The thicknesses of the passive waveguides D are therefore always needed to be

smaller than the critical D_c, which depends on the structure of the active waveguide.

As discussed above, for coupled waveguide lasers, the beam divergence is improved because the far field is modulated by the presence of the passive waveguides. To make the modulation of the far field efficient, the modulation factor can not be too small and the separation between waveguides needs to be large enough. However, a large separation S reduces the coupling strength and then reduces the modulation factor. To obtain a large modulation factor and a large separation S simultaneously, the thickness D of the passive waveguide therefore should be chosen so that the beam divergence changes slowly with the increase of C (see Fig. 4). A better chosen D is the one which is close to the critical thickness, D_c. However, when D approaches D_c the threshold current density increases rapidly [see Fig. 6(a)]. A compromise has to be made. A good compromise would be for C not too small and D not too close to D_c. From Fig. 6(a) and 6(b), we can find that the desired D should be about 1000 Å and the desired C should be larger than 8000 Å. However, for a good far-field pattern, the separation between waveguides, S, can not be too large because of the appearance of side lobes and the tightness of design tolerance. A suitable choice for C is 8000 Å. Because the separation between waveguides can not be small (for a good beam divergence), the electric field should not be bound too tightly in the active waveguide in order to obtain a sufficient coupling between waveguides. This is why we choose the active waveguide with $x = 0.4$ and $B = 800$ Å in this study rather than that with $x = 0.6$ and $B = 1500$ Å which has a larger confinement factor and a lower threshold current density (see Fig. 3). On the other hand, the active waveguide which confines the electric field too loosely should also be avoided because of the increase of the threshold current density. Once the active waveguide is determined, we have simultaneously determined $n_{\text{eff}2}$ and D_c. According to the discussion above, the other parameters can then be chosen properly.

From the calculated results and the discussion above, we can propose an InGaAs–AlGaAs coupled waveguide laser structure for 980 nm applications. It is the structure with a 65 Å $In_{0.2}Ga_{0.8}As$ quantum well, 150 Å GaAs barriers (region A), 800 Å graded layers (region B) linearly graded from GaAs to $Al_{0.4}Ga_{0.6}As$, 8700 Å $Al_{0.4}Ga_{0.6}As$ region C, 1000 Å GaAs passive waveguides (region D), and a longitudinal cavity length of 1 mm. The threshold current density for this structure is expected to be 160 A/cm^2 and the FWHM is 21° with a good far-field pattern (see Fig. 7). It should be point out that the laser structure with the record FWHM of 11.2° is not the desired one for the coupling application because of the serious side lobes and the high threshold current density [13]. Other structures with small FWHM's are also found to have the threshold current density much higher than that for our proposed structure.

In this study, we have assumed a single passive waveguide in each cladding layer. For structures with multiple passive waveguides in each cladding layer [13], the analysis for both the threshold current density and the beam divergence is similar to that presented in this study. The formula (18) for the far-field pattern will contain more terms of the cosine functions. We have also assumed that the waveguides are isolated from the cap layer, metal layer, and the substrate. In reality, these layers may influence the performance of lasers, regardless of whether they are the coupled waveguide lasers or the conventional GRINSCH lasers, if the separations between these layers and the active waveguide are not large enough.

V. Conclusion

We have theoretically investigated both the threshold current density and the beam divergence for coupled waveguide lasers using couple mode theory. The coupled waveguide structure is composed of an active waveguide which provides gain and two passive subordinate waveguides used to modulate the far-field pattern. The theoretical results show that the far-field pattern for the coupled waveguide laser depends on the modulation factor and the separation between the waveguides. Based on our analysis, the beam divergence can be significantly improved using the coupled waveguide structure with only a slight increase of the threshold current density.

Exact numerical calculation for coupled waveguide structures has been performed. Results from calculation are well interpreted using the simple coupled mode theory. The thicknesses of the passive waveguides are required to be thinner than a critical thickness for the fundamental mode operation. The separation between waveguides needs to be large enough, and, the coupling needs to be strong enough to make the modulation of the far-field efficient. Therefore, the width of the passive waveguides should approach the critical width so that the modulation factor converges slowly to zero with the increase of the separation between waveguides. Large separation between waveguides should be avoided because the side lobes may appear in the far-field pattern. A long optical cavity is required to obtain the insensitivity of the threshold current density to the coupling between waveguides. An optimum 980-nm InGaAs–AlGaAs coupled waveguide laser structure is proposed. It has a low threshold current density of 160 A/cm^2 and a small FWHM of 21° with a good far-field pattern.

References

[1] H. Horikawa and A. Ishii, "Semiconductor pump laser technology," *J. Lightwave Technol.*, vol. 11, pp. 167–175, 1993.

[2] N. Chand, E. E. Becker, J. P. van der Ziel, S. N. G. Chu, and N. K. Dutta, "Excellent uniformity and very low (<50 A/cm^2) theshold current density strained InGaAs quantum well diode lasers on GaAs substrate," *Appl. Phys. Lett.*, vol. 58, pp. 1704–1706, 1991.

[3] R. L. Williams, M. Dion, F. Chatenoud, and K. Dzurko, "Extremely low threshold current strained InGaAs/AlGaAs lasers by molecular beam epitaxy," *Appl. Phys. Lett.*, vol. 58, pp. 1816–1818, 1991.

[4] N. C. Frateschi, J. S. Osinski, C. A. Beyler, and P. D. Dapkus, "Low-threshold single-quantum-well InGaAs/GaAs lasers grown by metal-organic chemical vapor deposition on structured substrates," *IEEE Photon. Technol. Lett.*, vol. 3, pp. 209–212, 1992.

[5] M. Okayasu, M. Fukuda, T. Takeshita, and S. Uehara, "Stable operation (over 5000 h) of high-power 0.98-μm InGaAs-GaAs strained quantum well ridge waveguide lasers for pumping Er^{3+}-doped fiber amplifiers," *IEEE Photon. Technol. Lett.*, vol. 2, pp. 689–691, 1990.

[6] Y. K. Chen, M. C. Wu, W. S. Hobson, S. J. Pearton, A. M. Sergent, and M. A. Chin, "High-power 980-nm AlGaAs/InGaAs strained quantum-well lasers grown by OMVPE," *IEEE Photon. Technol. Lett.*, vol. 3, pp. 406–408, 1991.
[7] A. Moser, A. Oosenbrug, E. E. Latta, Th. Forster, and M. Gasser, "High-power operation of strained InGaAs/AlGaAs single quantum well lasers," *Appl. Phys. Lett.*, vol. 59, pp. 2642–2644, 1991.
[8] H. C. Casey, Jr. and M. B. Panish, *Heterostructure Lasers, Part A.* New York: Academic, 1978, p. 20.
[9] M. C. Wu, Y. K. Chen, M. Hong, J. P. Mannaerts, M. A. Chin, and A. M. Sergent, "A periodic index separate confinement heterostructure quantum well laser," *Appl. Phys. Lett.*, vol. 59, pp. 1046–1048, 1991.
[10] T. M. Cockerill, J. Honig, T. A. DeTemple, and J. J. Coleman, "Depressed index cladding graded barrier separate confinement single quantum well heterostructure laser," *Appl. Phys. Lett.*, vol. 59, pp. 2694–2696, 1991.
[11] A. C. Crook, C. M. Herzinger, T. M. Cockerill, D. V. Forbes, J. Honig, T. A. DeTemple, J. J. Coleman, I. A. White, and P. A. Besse, "Modal properties of depressed cladding semiconductor waveguides and lasers," *IEEE J. Quantum Electron.*, vol. 30, pp. 2817–2826, 1994.
[12] Y. C. Chen, R. G. Waters, and R. J. Dalby, "Single quantum well laser with vertically integrated passive waveguides," *Appl. Phys. Lett.*, vol. 56, pp. 1409–1411, 1990.
[13] ——, "Single quantum-well laser with 11.2 degree transverse beam divergence," *Electron. Lett.*, vol. 26, 1348–1350, 1990.
[14] A. Yariv, "Coupled mode theory for guided wave optics," *IEEE J. Quantum Electron.*, vol. QE-9, pp. 919–933, 1973.
[15] J. Buus, W. J. Steward, J. Haes, J. Willems, and R. G. Baets, "Spot size expansion for laser-to-fiber coupling using an integrated multimode coupler," *J. Lightwave Technol.*, vol. 11, pp. 582–588, 1993.
[16] D. C. Liu, C. P. Lee, C. M. Tsai, T. F. Lei, J. S. Tsang, W. H. Chiang, and Y. K. Tu, "Role of cladding layer thicknesses on strained-layer InGaAs/GaAs single and multiple quantum well lasers," *J. Appl. Phys.*, vol. 73, pp. 8027–8034, 1993.
[17] Y. C. Chen, P. Wang, J. J. Coleman, D. P. Bour, K. K. Lee, and R. G. Waters, "Carrier recombination rates in strained-layer InGaAs-GaAs quantum wells," *IEEE J. Quantum Electron.*, vol. 27, pp. 1451–1454, 1991.
[18] J. Buus, "Beamwidth for asymmetric and multilayer semiconductor laser structures," *IEEE J. Quantum Electron.*, vol. 17, pp. 732–736, 1981.

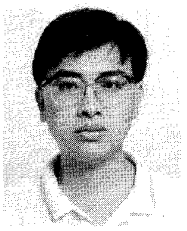

Shun Tung Yen (S'94) was born in Penghu, Taiwan, in 1969. He received the B.S. degree in Electronics Engineering from National Chiao Tung University, Hsinchu, Taiwan, in 1992, and is currently a Ph.D. student at the Department of Electronics Engineering of National Chiao Tung University.

His research interestings include the physics of optoelectronic devices and semiconductor microstructures.

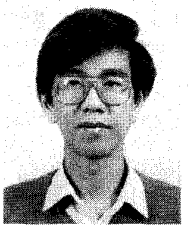

Chien Ping Lee (M'80–SM'94) received the B.S. degree in physics from National Taiwan University in 1971 and the Ph.D. degree in applied physics from California Institute of Technology in 1978.

While at Caltech, he worked on GaAs-based integrated optics. He was credited with the design and fabrication of several important optoelectronic components, including the first integrated optoelectronic circuit, which consists of a laser and a Gunn device fabricated on a same substrate. After graduation, he joined Bell Laboratories, where he worked on integrated optics and semiconductor lasers. He joined Rockwell International in 1979 and worked on GaAs integrated circuits. He did extensive work on substrate related effects such as the orientation effect and the backgating effect. In 1987, he joined National Chiao Tung University in Taiwan as professor and director of the Semiconductor Research Center. In 1990, he went back to Rockwell and was manager of the advanced device concept department. He came back to Taiwan in 1992 and is currently professor in the Institute of Electronics of National Chiao Tung University. His research interests are in the areas of III–V optoelectronic devices, MBE technology, GaAs IC's, heterostructure devices and physics, and device simulation.

Dr. Lee received the Engineer of the Year award in 1982 for his contribution in GaAs IC and HEMT technologies. He also received the best teacher award from the Ministry of Education in 1993 and the outstanding research award from the National Science Council in 1994.